Revealing Trap States in Lead Sulphide Colloidal Quantum Dots by Photoinduced Absorption Spectroscopy

Kahmann, Simon; Sytnyk, Mykhailo; Schrenker, Nadine; Matt, Gebhard J.; Spiecker, Erdmann; Heiss, Wolfgang; Brabec, Christoph J.; Loi, Maria A.

Published in:
Advanced electronic materials

DOI:
10.1002/aelm.201700348

Publication date:
2018

ADVANCED ELECTRONIC MATERIALS
www.advelectronicmat.de

Revealing Trap States in Lead Sulphide Colloidal Quantum Dots by Photoinduced Absorption Spectroscopy

*Simon Kahmann, Mykhailo Sytnyk, Nadine Schrenker, Gebhard J. Matt, Erdmann Spiecker, Wolfgang Heiss, Christoph J. Brabec, and Maria A. Loi**

Due to their large surface to volume ratio, colloidal quantum dots (CQDs) are often considered to exhibit a significant amount of surface defects. Such defects are one possible source for the formation of in-gap states (IGS), which can enhance the recombination of excited carriers, i.e., work as electrical traps. These traps are investigated for lead sulphide CQDs of different size, covered with different ligands using a mid-infrared photoinduced absorption (PIA) technique. The obtained PIA spectra reveal two distinct absorption bands, whose position depends on the particle size, i.e., the electronic confinement in the CQDs. Smaller particles exhibit deeper traps. The chemical nature of the capping ligand does not affect the resulting position other than due to its change in confinement, but better passivating species lead to smaller signals. Furthermore, ligand specific narrow lines observed are superimposed on the broad electronic background of the PIA spectra, which is attributed to Fano resonances caused by the interplay of the narrow molecular vibrations and the continuum of trap states. Mid-infrared photoinduced absorption represents a valuable tool to unravel distributions of IGS in CQDs and allows for an assessment of the quality of ligand exchanged films. These findings have implications for understanding the performances of CQD-based (opto-) electronic devices, such as solar cells, transistors, or quantum dot light emitting diodes, which are limited by frequent carrier trapping events.

1. Introduction

Colloidal quantum dots (CQDs) are often based on either II–VI or VI–VI semiconductors–predominantly cadmium or lead chalcogenides (PbX, CdX). These classes of materials are highly attractive for applications in the field of (opto-)electronics– mostly due to the feasible processing from solution and the tunability of their bandgap energy. Lead sulphide (PbS), in particular, attracts considerable interest due to its narrow bulk bandgap of 0.41 eV and the subsequent possibility to harness infrared photons in detectors and solar cells[1–4] or emit infrared light.[5–7]

As-synthesized CQDs are commonly covered with long, electrically insulating surface ligands that need to be exchanged in order to promote electrical conduction. This exchange improves the charge carrier mobility, but can simultaneously affect the quantum dot (QD) density of states (DOS) and may introduce in-gap states (IGS).[8] In most cases, IGS are considered as trap states. The high surface to volume ratio renders the CQDs vulnerable to surface-related defects, which might be caused by incomplete surface passivation, surface oxidation, or interfacial states caused by the attachment of exchanged ligands. Such defect states were observed for PbS before by various techniques. Reported were especially a state 0.2 eV above the valence level of 1,2-ethanedithiol or 1,3-mercaptopropionic acid (EDT, MPA) capped CQDs via Kelvin probe force microscopy (KPFM) and scanning tunneling spectroscopy (STS),[9–12] Additionally, a quasimetallic midgap band ≈0.4 eV below the conduction

S. Kahmann, Prof. M. A. Loi
Photophysics and OptoElectronics Group
Zernike Institute of Advanced Materials
University of Groningen
Nijenborgh 4, Groningen 9747 AG, The Netherlands
E-mail: m.a.loi@rug.nl

The ORCID identification number(s) for the author(s) of this article can be found under https://doi.org/10.1002/aelm.201700348.

DOI: 10.1002/aelm.201700348

S. Kahmann, Dr. G. J. Matt, Prof. C. J. Brabec
Institute for Materials in Electronics and Energy Technology (i-MEET)
Friedrich-Alexander Universität Erlangen-Nürnberg
Martensstraße 7, Erlangen 91058, Germany

Dr. M. Sytnyk, Prof. W. Heiss
Institute for Materials in Electronics and Energy Technology (i-MEET)
Friedrich-Alexander Universität Erlangen-Nürnberg
Energy Campus Nürnberg
Füher Straße 250, Nürnberg 90429, Germany

N. Schrenker, Prof. E. Spiecker
Center for Nanoanalysis and Electron Microscopy (CENEM)
Friedrich-Alexander Universität Erlangen-Nürnberg
Cauerstraße 6, Erlangen 91058, Germany

Prof. C. J. Brabec
Bavarian Center for Applied Energy Research (ZAE-Bayern)
Immerwahrstraße 2, Erlangen 91058, Germany

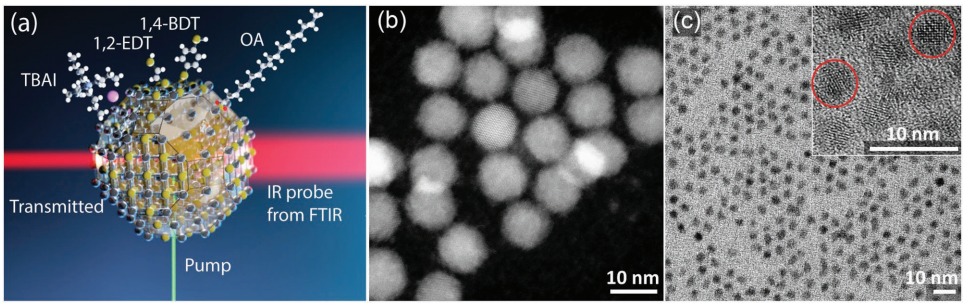

Figure 1. Sketch of the pump-probe measurement including the different ligands covering the PbS CQD surface. a) HRSTEM image of large b) and HRTEM image of small CQDs with a magnification in the inset c).

level for EDT capped PbS was reported for electron transport experiments.[13,14] For PbS treated with tetrabutylammonium iodide (TBAI) a trap distribution with an activation energy of 0.34 eV was found via temperature-dependent impedance spectroscopy.[15]

Using optical pump-probe spectroscopy, the groups of Asbury and Sargent observed a broad photoinduced absorption (PIA) around 0.3 eV with a long lifetime (still visible after 200 µs) for a range of ligands, including EDT and MPA, and attributed this observation to surface trap states.[16,17] Bakulin et al. finally reported two distributions, independent of each other, at activation energies of 0.2 and 0.3–0.5 eV for EDT and MPA capped PbS, distinguishable by their lifetimes.[18]

The corruption of a clean bandgap via ligand exchanging was furthermore related to the emergence of photoluminescence (PL) at energies below the direct bandgap transition.[4,19–21] Indeed, these works underlined that these states lead to a significant reduction in open circuit voltage and thereby overall solar cell efficiency.[21,22] A clear understanding of these IGS and how to suppress them is thus crucial for further improvement of these materials for future applications.

Most aforementioned reports share that at maximum two different ligands and only a single particle size were studied. Additionally, the energy resolution–when available–was limited and no attempt was made to investigate the precise shape of the IGS signatures.

In this work, we use a steady-state mid-infrared (MIR) pump-probe technique to investigate the PIA of PbS CQDs covered with several different ligands (**Figure 1**a for a scheme). This technique not only offers a high energy resolution, but also allows to illuminate a broad sample area at low light intensity, thus reducing negative side effects such as sample degradation or higher order processes. This steady state technique furthermore offers information about the equilibrium state that allows for comparison to the results obtained via KPFM or STS. In addition to the native oleic acid (OA), we employ shorter organic ligands such as EDT and 1,4-benzenedithiol (BDT) as well as TBAI, i.e., ligands commonly employed in (opto-) electronic devices[20,23–25] and examine the impact on the PIA response also as a function of mean particle size.

For all samples examined, a broad photoinduced absorption emerges in the MIR spectral region. This absorption consists of two partially overlapping bands that shift toward lower energy for narrower bandgaps. The signal strength increases when exchanging the native OA to TBAI, EDT or BDT. We consequently ascribe both absorption bands to surface-related trap states within the CQD bandgap. Finally, we examine the molecular vibrations of the ligands and observe that for BDT and OA narrow lines in the PIA spectra coincide with their molecular vibrations. We attribute these lines to a Fano resonance occurring between the narrow molecular vibration and the continuum of trap states.

2. Results and Discussion

We investigated the CQDs when covered with their native OA or with shorter entities (BDT, EDT, and TBAI; see Experimental Section for ligand exchange protocol)–their respective structure is displayed in Figure 1a. Three differently sized CQDs were considered in this investigation (small: first excitonic peak in toluene at 1.24 eV; medium: 1.11 eV; and large: 0.76 eV; Figure S1, Supporting Information). The approximate size range can be inferred from the position of the excitonic peak, but to more precisely determine the size and shape of these CQDs, we took high resolution electron microscopy (HRSTEM and HRTEM) images as depicted in Figure 1b,c. The large particles in (b) exhibit a highly regular shape with a mean particle size of 10.6 nm, as determined from the selected area diffraction pattern (Figure S2a, Supporting Information). The small particles (4.2 nm; Figure 1c and Figure S2b, Supporting Information) similarly exhibit a regular shape with clearly discernible crystal planes as depicted in the inset and thereby underlining our high material quality.

Pump-probe measurements were carried out at 77 K, unless stated otherwise, to improve the signal to noise ratio. The spectral features were determined to be independent of the excitation energy and all spectra depicted in the following were taken under excitation at 1.6 eV (780 nm). **Figure 2** presents the results for small, medium, and large PbS when covered with the different ligands. Each spectrum displays a broad region of photoinduced absorption below 0.5 eV that consists of two clearly resolvable, but overlapping, bands. These bands shift significantly from ≈0.2 and 0.4 eV for small CQDs down to 0.1–0.2 eV for large CQDs. For a larger bandgap, the PIA bands are hence also found at larger energy (also consider Figure 2d or Figure S3a, Supporting Information). Some of the samples exhibit narrow features superimposed on the broad bands, which we shall discuss separately farther below. Comparing the different ligands for the same particle size, one finds that the formation of two distinct bands is common to all investigated

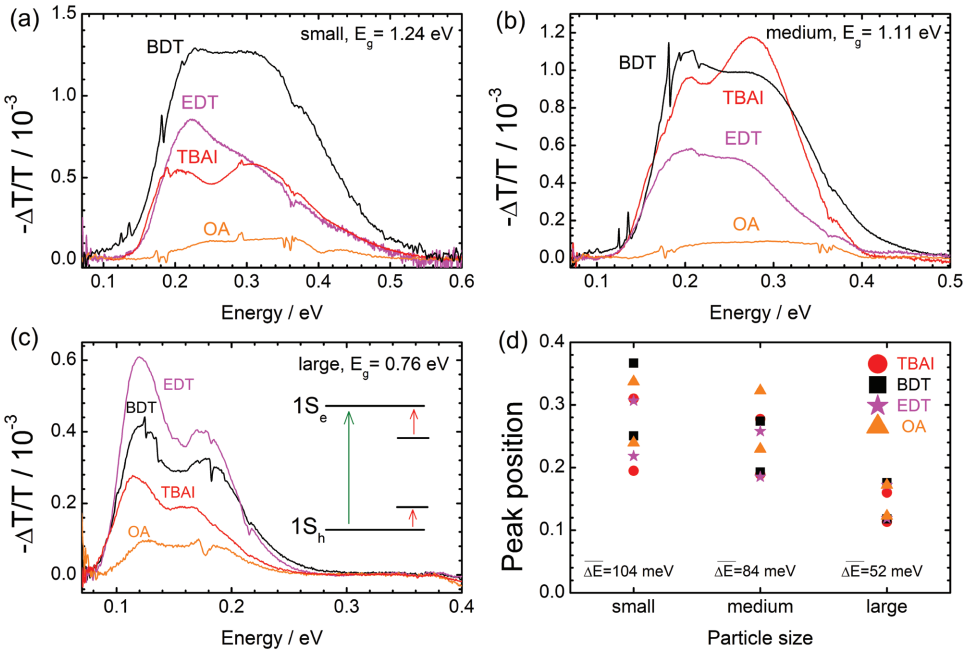

Figure 2. PIA spectra for films of small a), medium b), and large c) CQDs capped with different ligands upon excitation with 1.6 eV light. The energy of their first excitonic peak is indicated to estimate the trap depth. Peak position of the fitted Gaussian distributions for each spectrum in (a–c) with values denoting the average peak separation for each particle size d). The sketch in the inset of (c) depicts the excitation of the CQD in green and the re-excitation of trapped carriers in red.

samples and no additional signals arise or vanish due to ligand variation. We consequently fitted all curves using two Gaussian peaks (Figure S5, Supporting Information shows examples) and present the obtained peak energies and widths in Table S1 (Supporting Information). Interestingly, TBAI treated PbS and large CQDs in general lead to narrower distributions, which correlate with their film absorption spectra as depicted in Figure S4 (Supporting Information). We therefore conclude that small variations in PIA shape and position are not due to the capping ligands (i.e., their chemical nature) themselves, but are evoked by changes in confinement, i.e., the average bandgap energy and variance thereof.

We furthermore determined the separation of the two peaks for each sample as plotted in Figure 2d (Table S1, Supporting Information for values) and find that it significantly increases for smaller particles (i.e., larger bandgap). Finally, we would like to note that these signals are also observable when measuring at room temperature as depicted in Figure S3b (Supporting Information), but become less pronounced.

Photoinduced transitions in this energy region may be explained by higher excitations from already excited CQDs,[26] e.g., lifting an electron from the $1S_e$ to the $1P_e$ level. In case of still bound excitons, this would lead to a small signal in a steady state measurement and generally to an increased signal for CQDs with larger exciton lifetime—contrary to what is observed. Free charge carriers could be a more likely candidate,[27] given their longer lifetime. One might assume that free electrons and free holes formed in the CQD films to be responsible for the two distinct absorption bands. Free carrier formation is promoted by shorter ligands and would therefore explain the increased signal strength upon ligand exchange. Key aspects discussed below, however, allow us to dismiss this model. We furthermore dismiss the Drude response of free charge carriers as the origin, as in this case we would expect a continuously increasing signal toward low energy instead of two distinct bands shifting with particles size. The bands are consequently assigned to surface trap states within the bandgap, leading to trap-to-band transitions as depicted in the inset of Figure 2c. In this picture, the well passivating native OA suppresses the formation of such states and exchanging it leads to an increased density of traps, hence photoinduced absorption. Corroborating this claim, we observe an increased PL from energies lower than the bandgap for ligand exchanged CQDs (Figure S6, Supporting Information), which, in accordance to several reports in the literature, we explain as trap-induced emission.[4,19–21] Moreover, large CQDs, with their smaller surface to volume ratio and longer reaction time, are considered to exhibit a lower surface trap density, which we observe as a distinctly lower PIA signal for all employed ligands. This effect would not be explained by assuming intraband transitions to be responsible for the absorption bands. In agreement with the proposed trap-to-band mechanism, we also observe a saturation of the peak intensity for increasing pump power density (displayed in Figure S7, Supporting Information), which we ascribe to trap filling.

We turn to further experiments that offer additional information on the origin of these states. To exclude spurious processes during ligand exchange, we only investigated CQDs covered with native OA in further detail. As reported in Figure 2, the PIA for these samples is significantly lower than for the exchanged ones, but the absorption bands still form distinctively. To find the origin of the trap states in PbS CQDs, we examined a sample (small CQDs) that was stored under environmental conditions for an entire year. The comparison with the fresh material in **Figure 3**a reveals an increased signal and

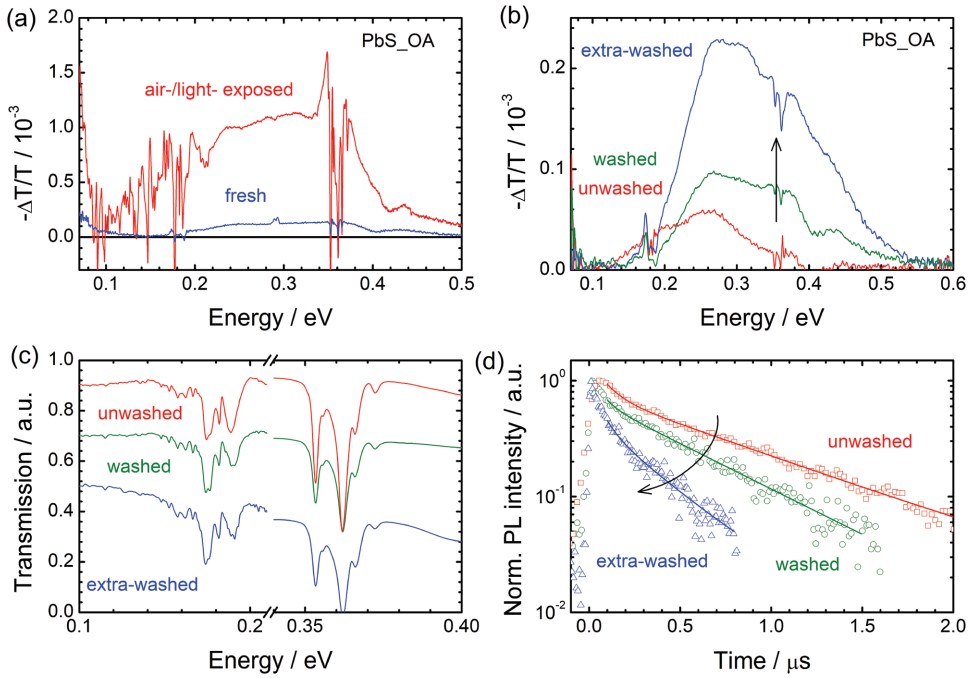

Figure 3. PIA spectra of freshly prepared PbS_OA and after environmental exposure for a year a). PIA spectra of PbS_OA films before and after several washing b) with their respective transmission spectra c). The higher energy absorption band is not formed prior to the first washing. The transients in (d) exhibit a steady decrease of PL lifetime with the number of washing steps.

more pronounced narrow features. Whereas air exposure, leading to oxygen adsorption, was linked to the creation of trap states before,[11] it was pointed out that this adsorption was reversible under vacuum. Given the extended sample storage under high vacuum prior to the measurement (at least 12 h), the amount of adsorbed oxygen in our experiments should be negligible. These small CQD dramatically change their shape and become irregular while maintaining their crystalline core as demonstrated by the HRTEM image (Figure S8, Supporting Information), which shows a pronounced surface reconstruction. A probable explanation for the increased signal would thus be the removal of bound ligands. This observation is also a key argument to favor trap-to-band transition as opposed to intraband transitions of free charge carriers as the origin of the PIA signals.

Assuming thus the degree of ligand coverage to affect the PIA spectra, we next investigated the behavior of small PbS_OA as a function of postsynthesis washing. As displayed in Figure 3b, as-synthesized (unwashed) CQDs do not exhibit any absorption at 0.36 eV–only the lower energy absorption band is weakly present. For our "normal" washing (four cycles after synthesis, consider the Experimental Section for details) and the more extensive washing (11 cycles), both absorption bands are formed and the signal strength increases with the number of washing steps. This trend agrees well with our previous observations of a decreasing J_{SC} in CQD solar cells, attributed to trap mediated recombination, upon excessive postsynthesis washing[23] and this behavior again refutes the model of intraband transitions, e.g., one being due to electrons and the other due to holes. As expected, the surface chemistry of OA ligands does not change upon washing (normalized transmission spectra in (c)). Underpinning aforementioned trends of steady increase in PIA signal strength and J_{SC} in solar cells, the transient PL, depicted in (d), exhibits a lifetime reduction upon increased washing.

Concluding the first part of our investigation, we find two separate trap states in the bandgap of PbS CQDs that shift toward higher energies for larger bandgap CQDs and include the energy regions reported before (when carried out on sizes corresponding to our "small" or "medium"). The observation of two distinct distributions may explain why some groups reported states close to the valence level and others associated them with the conduction level.[9–14,28]

The surface chemistry of PbS CQDs is more complex than simple schemes such as the one in Figure 1a suggest. Even as-synthesized CQDs do not only exhibit two differently polarized crystal facets ((001) and (111)), but are also covered with hydroxyl and oleate ions additional to oleic acid.[29] Kim et al. furthermore suggested that besides to defects, IGS were related to the overall stoichiometry of the QD surface.[8] We thus deem it likely that washing and the concomitant stripping of ligands may not only lead to a change in degree of surface coverage, but also of surface composition, which in turn affects the partial charges of Pb and S atoms on the CQD surface. Especially the energy region around 0.37 eV (for small particles) was previously linked to elemental Pb^0 in CQDs.[30] Similarly, the exposure of oxygen was proposed to lead to a remodeling of the surface structure and change of the local Pb:S ratio.[31] In this light, it seems plausible that a prolonged exposure to air leads to an extended surface remodeling as observed in Figure S8 (Supporting Information), which in turn leads to a stronger PIA signal.

We therefore propose that further theoretical studies focusing on the impact of the Pb and S oxidation states on the

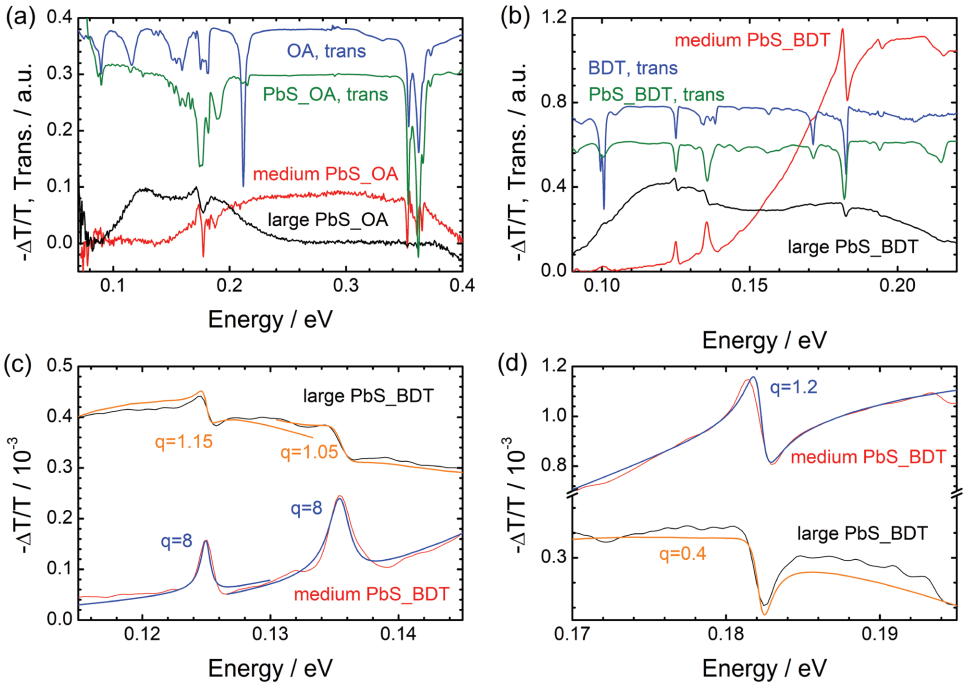

Figure 4. Transmission spectra of the pristine ligands and when capping PbS CQDs and the respective PIA spectra for small and medium PbS for OA a) and BDT b). Inset of the low energy region of the PbS_BDT PIA spectra with Fano profiles fitted to the pronounced narrow features.

DOS are a promising route to a deeper understanding of the trap formation.

In the following, we focus on the narrow features superimposed on the broad PIA bands observable for OA and BDT. Comparable signals were noted before, but not further analyzed.[16,17] The low energy transmission spectra of neat OA, PbS_OA, and the corresponding PIA spectra for medium and large particles are depicted in **Figure 4**a. As stated above, OA deprotonates to bind in its oleate form (OA^-) to surface Pb^{2+} on the polar (111) facet and OA bidentately bridges Pb and S atoms on the (001) facet.[17,29] The deprotonation of OA is apparent by the emergence of two broad absorption bands around 0.185 eV (1500 cm^{-1}) in Figure 4a, which are due to the symmetric and asymmetric stretch vibrations of the anchoring carboxyl group (Table S3, Supporting Information). In the PIA spectra, narrow features are observable both in the region of methyl- and methylene (CH_x) vibrations slightly below 0.36 eV (3000 cm^{-1}) and for the COO^- vibrations around 0.185 eV. Strikingly, however, the carboxyl features are only observable for the medium (and small) sized CQDs, where the features energetically coincide with the trap induced PIA band.

In case of BDT, as depicted in Figure 4b, most of the features of unattached ligands coincide with those of PbS_BDT, but some absorption lines are significantly weaker for the latter–especially those at 0.1 and 0.17 eV (800 and 1380 cm^{-1}). Although the BDT molecule is assumed to remain chemically unchanged upon binding to PbS CQDs, the attachment can change dipole moments in the environment and reduce the molecule's symmetry. Consequently, oscillator strengths and resonant energies may change. Figure 4b displays that also for BDT, all narrow features in the PIA spectra coincide perfectly with molecular vibrations. The shape of these features, however, is drastically different for the two particle sizes (at the same energy) and also varies for the same size (at different energies).

Such features could in principle be caused by the Stark effect, i.e., by the electrical field of trapped charges acting on the resonant frequency of the molecular vibrations of attached ligands. As we discuss in more detail in the Supporting Information, the Stark effect fails to explain why for the PbS_BDT the shape of the narrow features changes for different particle sizes and why PbS_OA only exhibits narrow features for small CQDs.

We propose, in contrast, that these features are due to Fano resonances.[32,33] In order for this effect to occur, a narrow vibration needs to interact with an energetically broad process that coincides energetically. The resulting Fano profile has the form of $FP = \frac{(\varepsilon + q)^2}{\varepsilon^2 + 1}$, where q is a phenomenological shape parameter and ε is the reduced energy defined as $\varepsilon = \frac{2(E - E_F)}{\Gamma}$. E_F is the resonant energy of the Fano process and Γ is the width of the narrow vibration (consider Figure S10, Supporting Information for different Fano profiles).

Using this profile, we sought to model the three most pronounced narrow features for PbS_BDT between 0.12 and 0.19 eV (consider the Supporting Information for a detailed explanation and Table S2, Supporting Information for the data). As depicted in Figure 4c,d, our model yields a remarkable agreement with the experimental data. As indicated, the q-parameter employed is large when the molecular vibration and the peak of the trap distribution are widely separated and approaches zero when they almost coincide. This fits the interpretation of q as a measure for their interaction. In case of a large q, this is weak.

When q is around 1, the continuum transition and the narrow vibration are of the same strength.

Accordingly, the absence of narrow features around 0.36 eV for large PbS_OA is explained by the absence of a continuous state at that energy.

To precisely understand why only some of the vibrations lead to features in the PIA spectra is beyond the scope of this work, we think, however, that a more thorough understanding of the mechanisms will ultimately offer more fundamental insight into the nature of ligand binding to surface atoms. Notably, all of the PbS_BDT PIA signals are related to the benzene ring vibrations and none to the anchoring -SH group (Table S4, Supporting Information). Accordingly, we do not observe any narrow features for PbS_EDT, despite a rich spectrum of molecular vibrations (Figure S9, Supporting Information).

3. Conclusion

In conclusion, we examined the mid-infrared photoinduced absorption of lead sulphide CQDs capped with ligands commonly applied for (opto-)electronic applications and observe two PIA bands which we ascribe to surface trap states. Whereas these two bands shift from ≈0.35 and 0.22 eV for CQDs, with a first excitonic peak around 1.2 eV, toward energies between 0.1 and 0.2 eV, for large diameter particles, with an excitonic peak around 0.8 eV, their position is not affected by the type of ligand attached to the surface. The energy region thus contains all values for trap- or in-gap states in PbS CQDs reported so far. We thus conclude that the variations found in literature are due to differently sized CQDs. The magnitude of the photoinduced bands changes upon exchanging the native oleic acid to shorter ligands. Similarly, extensive exposure to light and air do not affect the spectral features other than by increasing them. We thus associate these traps with the atoms inherent in the CQDs rather than interface states caused by the binding of surface ligands. Our data furthermore allow to dismiss the assumption of these bands to be due to intraband transitions of free charge carriers.

The PIA technique employed herein is hence a viable tool for assessing the quality of the surface passivation of CQDs–a crucial aspect for further optimization of future device performance.

For CQDs covered with BDT or OA, narrow features are additionally observed in the PIA spectra, which can be connected to the ligands' molecular vibrations. We explain their emergence as Fano type resonances occurring between molecular vibrations and the continuous trap band.

4. Experimental Section

Chemicals: 99.999% lead oxide (PbO), OA, 1-octadecene (ODE), and hexamethyldisilathiane (HMDT) were received from Sigma-Aldrich. Anhydrous toluene, *n*-hexane, and ethanol were bought from Alfa Aesar. All chemicals were used as received.

Synthesis of PbS QDs: PbS QDs were synthesized analogously to previous reports.[34] Briefly, a lead oleate precursor was prepared in situ by dissolving PbO in OA/ODE mixture under vacuum at 130 °C for 1 h. The sulphur precursor solution was prepared through dissolving HMDT in dried ODE and was rapidly injected into vigorously stirring lead oleate under argon (Pb/S molar ratio was 2:1.7) at 150 °C. After self-cooling of the mixture down to room temperature, ODE was added followed by washing steps, which were carried out via precipitation with anhydrous ethanol, centrifugation at 8000 rpm and redispersion in anhydrous *n*-hexane. The QDs are eventually dissolved in anhydrous toluene. From 4 to 11, washing steps were applied.

TEM Analysis: For transmission electron microscopy (TEM) analysis, the PbS nanoparticle solution was coated onto a thin carbon film. HRTEM and HRSTEM images of large and aged particles were taken at a double-corrected FEI Titan Themis^3 300 at 200kV. Selected area diffraction patterns were taken at a Philips CM300 UT at 300 kV. The mean nanoparticle size was determined from the diffraction patterns by applying the Scherrer equation using a shape factor of $K = 0.89$ for spheres. The images for the small particles when fresh were obtained using a JEOL 2011 FasTEM microscope operating at an accelerated voltage of 200 kV.

PIA Measurement: Thin films were spin-cast from solution (hexane) on ZnSe platelets in a layer-by-layer fashion. The ligand treatment included soaking the as-cast layer for 1 min in the ligand-to be (BDT: 2.8 mg ml^{-1} in MeCN, EDT: 0.01 vol% in MeCN, and TBAI: 10 mg mL^{-1} in MeOH) with an additional cleaning step using the pristine solvent.

The substrates were subsequently mounted into a cryostat without having been exposed to air (if not stated otherwise) and brought into the beam path of the Bruker Vertex 70 FTIR spectrometer. The broad band mid-infrared beam was detected with a liquid nitrogen-cooled MCT detector. The employed beamsplitter in the interferometer is made of KBr. The sample, cooled down to 77 K, is excited by the 780 nm pump laser.

To avoid perturbations from the pump light, we furthermore installed a GaAs filter in front of the detector. Spectra were acquired with a resolution of 5 cm^{-1} and the following cycle was run at least 1024 times: first, the pump is switched on, followed by a delay of 1 s to establish equilibrium within the film, the "light on" spectrum is then measured 16 times and averaged. Next, the light is switched off, followed by another 1 s delay and 16 coadditions for the "light off" spectrum. The "light off" spectrum is also used as transmission measurement.

Power density dependent measurements were carried out using a set of neutral density filters. Since the narrow features were of no interest in this case, above outlined cycle was merely carried out 256 times.

Photoluminescence: The respective OA capped films were deposited on quartz substrates, sealed using epoxy glue, and excited at 400 nm using the second harmonic of a mode-locked Ti:sapphire laser (Mira 900) delivering pulses of 150 fs width at a repetition rate of ≈76 MHz. The Ti:sapphire laser was pumped by a solid-state Nd:vanadate (Nd:YVO4) diode laser, frequency doubled, thus providing a single-frequency green (532 nm) output at 5 W. Steady-state spectra were recorded with an InGaAs detector from Andor. Time-resolved traces were taken with a Hamamatsu streak camera working in single sweep mode. An optical pulse selector was used to vary the repetition rate of the exciting pulses.

Supporting Information

Supporting Information is available from the Wiley Online Library or from the author.

Acknowledgements

S.K. sincerely thank the Ubbo Emmius foundation and the research training group GRK 1896 of the German Research foundation for funding of his Ph.D. N.S. also acknowledges the GRK 1896 for funding of her Ph.D. M.S. and W.H. gratefully acknowledge the use of the services and facilities of the "Energie Campus Nürnberg" and financial support through the "Aufbruch Bayern" initiative of the State of Bavaria.

Conflict of Interest

The authors declare no conflict of interest.

Keywords

colloidal quantum dots, mid infrared spectroscopy, molecular vibrations, pump-probe spectroscopy, trap states

Received: July 28, 2017
Revised: October 30, 2017
Published online: December 5, 2017

[1] J. Gao, S. C. Nguyen, N. D. Bronstein, A. P. Alivisatos, *ACS Photonics* **2016**, *3*, 1217.
[2] C.-H. Chuang, P. R. Brown, V. Bulovic, M. G. Bawendi, *Nat. Mater.* **2014**, *13*, 796.
[3] X. Lan, O. Voznyy, F. P. Garcia de Arquer, M. Liu, J. Xu, A. H. Proppe, G. Walters, F. Fan, H. Tan, M. Liu, M. Z. Yang, S. Hoogland, E. H. Sargent, *Nano Lett.* **2016**, *16*, 4630.
[4] M. J. Speirs, D. N. Dirin, M. Abdu-Aguye, D. M. Balazs, M. V. Kovalenko, M. A. Loi, *Energy Environ. Sci.* **2016**, *9*, 2916.
[5] L. Sun, J. J. Choi, D. Stachnik, A. C. Bartnik, B.-R. Hyun, G. G. Malliaras, T. Hanrath, F. W. Wise, *Nat. Nanotechnol.* **2012**, *7*, 369.
[6] G. J. Supran, K. W. Song, G. W. Hwang, R. E. Correa, J. Scherer, E. A. Dauler, Y. Shirasaki, M. G. Bawendi, V. Bulovic, *Adv. Mater.* **2015**, *27*, 1437.
[7] X. Gong, Z. Yang, G. Walters, R. Comin, Z. Ning, E. Beauregard, V. Adinolfi, O. Voznyy, E. H. Sargent, *Nat. Photonics* **2016**, *10*, 253.
[8] D. Kim, D.-H. Kim, J.-H. Lee, J. C. Grossman, *Phys. Rev. Lett.* **2013**, *110*, 196802.
[9] Y. Zhang, D. Zherebetskyy, N. D. Bronstein, S. Barja, L. Lichtenstein, D. Schuppisser, L.-W. Wang, A. P. Alivisatos, M. Salmeron, *Nano Lett.* **2015**, *15*, 3249.
[10] Y. Zhang, Q. Chen, A. P. Alivisatos, M. Salmeron, *Nano Lett.* **2015**, *15*, 4657.
[11] Y. Zhang, D. Zherebetskyy, N. D. Bronstein, S. Barja, L. Lichtenstein, A. P. Alivisatos, L.-W. Wang, M. Salmeron, *ACS Nano* **2015**, *9*, 10445.
[12] B. Diaconescu, L. A. Padilha, P. Nagpal, B. S. Swartzentruber, V. I. Klimov, *Phys. Rev. Lett.* **2013**, *110*, 1.
[13] P. Nagpal, V. I. Klimov, *Nat. Commun.* **2011**, *2*, 486.
[14] D. Bozyigit, S. Volk, O. Yarema, V. Wood, *Nano Lett.* **2013**, *13*, 5284.
[15] Z. Jin, A. Wang, Q. Zhou, Y. Wang, J. Wang, *Sci. Rep.* **2013**, *6*, 37106.
[16] K. S. Jeong, J. Tang, H. Liu, J. Kim, A. W. Schaefer, K. Kemp, L. Levina, X. Wang, S. Hoogland, R. Debnath, L. Brzozowski, E. H. Sargent, J. B. Asbury, *ACS Nano* **2012**, *6*, 89.
[17] J. Tang, K. W. Kemp, S. Hoogland, K. S. Jeong, H. Liu, L. Levina, M. Furukawa, X. Wang, R. Debnath, D. Cha, K. W. Chou, A. Fischer, A. Amassian, J. B. Asbury, E. H. Sargent, *Nat. Mater.* **2011**, *10*, 765.
[18] A. A. Bakulin, S. Neutzner, H. J. Bakker, L. Ottaviani, D. Barakel, Z. Chen, *ACS Nano* **2013**, *7*, 8771.
[19] G. W. Hwang, D. Kim, J. M. Cordero, M. W. B. Wilson, C.-H. M. Chuang, J. C. Grossman, M. G. Bawendi, *Adv. Mater.* **2015**, *27*, 4481.
[20] C.-H. M. Chuang, A. Maurano, R. E. Brandt, G. W. Hwang, J. Jean, T. Buonassisi, V. Bulovic, M. G. Bawendi, *Nano Lett.* **2015**, *15*, 3286.
[21] A. Stavrinadis, S. Pradhan, P. Papagiorgis, G. Itskos, G. Konstantatos, *ACS Energy Lett.* **2017**, *2*, 739.
[22] M. J. Speirs, D. M. Balazs, H.-H. Fang, L.-H. Lai, L. Protesescu, M. V. Kovalenko, M. A. Loi, *J. Mater. Chem. A* **2015**, *3*, 1450.
[23] C. Piliego, L. Protesescu, S. Z. Bisri, M. V. Kovalenko, M. A. Loi, *Energy Environ. Sci.* **2013**, *6*, 3054.
[24] Z. Ning, O. Voznyy, J. Pan, S. Hoogland, V. Adinol, J. Xu, M. Li, A. R. Kirmani, J.-P. Sun, J. Minor, K. W. Kemp, H. Dong, L. Rollny, A. Labelle, G. Carey, B. Sutherland, I. Hill, A. Amassian, H. Liu, J. Tang, O. M. Bakr, E. H. Sargent, *Nat. Mater.* **2014**, *13*, 822.
[25] T. P. Osedach, N. Zhao, T. L. Andrew, P. R. Brown, D. D. Wanger, D. B. Strasfeld, L.-Y. Chang, M. G. Bawendi, V. Bulovic, *ACS Nano* **2012**, *6*, 3121.
[26] B. L. Wehrenberg, C. Wang, P. Guyot-Sionnest, *J. Phys. Chem. B* **2002**, *106*, 10634.
[27] K.-W. Jeong, P. Guyot-Sionnest, *ACS Nano* **2016**, *10*, 2225.
[28] M. I. Nugraha, R. Häusermann, S. Z. Bisri, H. Matsui, M. Sytnyk, W. Heiss, J. Takeya, M. A. Loi, *Adv. Mater.* **2015**, *27*, 2107.
[29] D. Zherebetskyy, M. Scheele, Y. Zhang, N. Bronstein, C. Thompson, D. Britt, M. Salmeron, A. P. Alivisatos, L.-W. Wang, *Science* **2014**, *344*, 1380.
[30] D. Zherebetskyy, L.-W. Wang, *J. Phys. Chem. Lett.* **2015**, *6*, 4711.
[31] F. Bertolotti, D. N. Dirin, M. Ibanez, F. Krumeich, A. Cervellino, R. Frison, O. Voznyy, E. H. Sargent, M. V. Kovalenko, A. Guagliardi, N. Masciocchi, *Nat. Mater.* **2016**, *15*, 987.
[32] U. Fano, *Phys. Rev.* **1961**, *124*, 18.
[33] M. F. Limonov, M. V. Rybin, A. N. Poddubny, Y. S. Kivshar, *Nat. Photonics* **2017**, *11*, 543.
[34] M. A. Hines, G. D. Scholes, *Adv. Mater.* **2013**, *15*, 1844.